

# The effect of beryllium oxide on retention in JET ITER-like wall tiles

C. Makepeace<sup>a,\*</sup>, C. Pardanaud<sup>b</sup>, P. Roubin<sup>b</sup>, I. Borodkina<sup>c,d</sup>, C. Ayres<sup>e</sup>, P. Coad<sup>e</sup>,  
A. Baron-Wiechec<sup>e</sup>, I. Jecu<sup>f</sup>, K. Heinola<sup>g</sup>, A. Widdowson<sup>e</sup>, S. Lozano-Perez<sup>a</sup>, J.E.T. Contributors<sup>h,1</sup>

<sup>a</sup> Department of Materials, University of Oxford, Parks Road, Oxford OX1 3PH, UK

<sup>b</sup> Aix-Marseille Université, CNRS, PIIM UMR 7345, 13397, Marseille, France

<sup>c</sup> National Research Nuclear University MEPhI, Moscow, 115409, Kashirskoe sh. 31, Russia

<sup>d</sup> Forschungszentrum Jülich GmbH, Wilhelm-Johnen-Strasse, 52428 Jülich, Germany

<sup>e</sup> CCFE, Culham Science Centre, Abingdon, OX14 3DB, UK

<sup>f</sup> National Institute for Laser Plasma and Radiation Physics, Bucharest-Magurele 077125, Romania

<sup>g</sup> University of Helsinki, PO Box 64, FI-00560 Helsinki, Finland

<sup>h</sup> EUROfusion Consortium, JET, Culham Science Centre, Abingdon, OX14 3DB, UK

## ABSTRACT

Preliminary results investigating the microstructure, bonding and effect of beryllium oxide formation on retention in the JET ITER-like wall beryllium tiles, are presented. The tiles have been investigated by several techniques: Scanning Electron Microscopy (SEM) equipped with Energy Dispersive X-ray (EDX), Transmission Electron microscopy (TEM) equipped with EDX and Electron Energy Loss Spectroscopy (EELS), Raman Spectroscopy and Thermal Desorption Spectroscopy (TDS). This paper focuses on results from melted materials of the dump plate tiles in JET. From our results and the literature, it is concluded, beryllium can form micron deep oxide islands contrary to the nanometric oxides predicted under vacuum conditions. The deepest oxides analyzed were up to 2-micron thicknesses. The beryllium Deuterioxide ( $\text{BeO}_x\text{D}_y$ ) bond was found with Raman Spectroscopy. Application of EELS confirmed the oxide presence and stoichiometry. Literature suggests these oxides form at temperatures greater than 700 °C where self-diffusion of beryllium ions through the surface oxide layer can occur. Further oxidation is made possible between oxygen plasma impurities and the beryllium ions now present at the wall surface. Under Ultra High Vacuum (UHV) nanometric Beryllium oxide layers are formed and passivate at room temperature. After continual cyclic heating (to the point of melt formation) in the presence of oxygen impurities from the plasma, oxide growth to the levels seen experimentally (approximately two microns) is proposed. This retention mechanism is not considered to contribute dramatically to overall retention in JET, due to low levels of melt formation. However, this mechanism, thought the result of operation environment and melt formation, could be of wider concern to ITER, dependent on wall temperatures.

## 1. Introduction

Beryllium is the material of choice for the International Thermonuclear Experimental Reactor (ITER) and therefore the subject of ongoing research surrounding fuel retention to meet ITER's safety case. Tritium, a radioactive isotope of hydrogen and one of two hydrogen isotopes used in the fusion reaction, has an operational safety limit of 700 g within the reactor vessel. The beryllium wall area, will equate to  $\sim 700 \text{ m}^2$ . Beryllium was chosen as the first wall cladding due to: reduced chemical erosion (compared to previous carbon counterparts); a high melting point; a low Z number; and good oxygen gettering from the plasma. The Joint European Torus (JET) moved to an ITER-like wall with beryllium limiters and a tungsten divertor in late 2010 and saw a factor of 20 reductions [1] of retained hydrogen isotopes compared to carbon walls. Since then three ITER-like wall campaigns have occurred producing reactor relevant materials for post mortem

analysis. This paper focuses on work from the first campaign and melted beryllium materials originating from the apex of JET which are compared against JET's midplane beryllium wall limiters tiles (which have not undergone melting). The apex of JET (the 'dump plate' tiles) is an area where comparably larger volumes of melted material are produced. Melted material appears to increase the propensity of beryllium oxidation, due to increased diffusion of beryllium to the surface, whereby oxygen from the plasma can react once more [2, 3]. Despite beryllium's often touted claim of 'good oxygen gettering', the result of oxidation on retention is widely discussed [4]. Data from controlled laboratory experiments lead to a complicated understanding of hydrogen retention and oxidation. The results are briefly summarized. Early reports from [5] found that both water and oxygen can independently oxidize beryllium to  $\sim 3$  monolayer thick islands. If both  $\text{H}_2\text{O}$  and oxygen are present coincidentally, further growth can occur to  $\sim 6$  monolayer depths [6,7]. However, formation of OH bonds at the

\* Corresponding author.

E-mail address: [carmen.makepeace@materials.ox.ac.uk](mailto:carmen.makepeace@materials.ox.ac.uk) (C. Makepeace).

<sup>1</sup> See the author list of "X. Litaudon et al. 2017 Nucl. Fusion 57 102001".

surface was not discovered. Retention decreased when oxidized beryllium was exposed to hydrogen, compared to clean beryllium [8]. Desorption of H occurred at 320 K for BeO surface and 450 K for the clean surface. Zalkind promoted oxide islands formation by nucleation at oxygen coverages above 2–3 monolayers, followed by lateral growth. Ion implantation was seen to double the oxygen sticking coefficient and increase the oxidation rate significantly [9]. Similarly, pre-adsorbed H significantly reduced the quantity of adsorbed oxygen on the surface. At  $T > 700^\circ\text{C}$  oxygen nucleates without chemisorption. Thermal desorption data, above all must be considered carefully [10]. The ease at which beryllium can oxidize, even under ultra-high vacuum conditions, has led authors to suggest samples were free of oxidation, when more likely partial oxide layers had already formed [11].

## 2. Experimental method

Tiles taken from the first ITER-like wall campaign (2011–12) were cut into individual castellations as previously described in [12] to avoid sample heating and produce thermal desorption relevant samples ( $1\text{ cm}^2 \times 250\text{ mm}$ ). All samples listed and discussed were originally 'maker layer' tiles designed to enable measurement of deposition and erosion. The tiles were prepared with bulk beryllium substrates upon which  $3\text{ }\mu\text{m}$  Ni and a further  $8\text{ }\mu\text{m}$  Beryllium (at the surface) were deposited with a thermionic vacuum arc [13,14]. Dump plate tiles orientated at the top of the vessel are indicated in Fig. 1; including the 2B2C dump plate photo (right) showing surface melting along the central ridge. For comparison, limiter tiles 2XR10 and 4D14 from the mid plane of the inner and outer walls respectively are also indicated in Fig. 1(a). A Tescan Mira XMH SEM equipped with an Oxford Instruments X-Max 80 EDS detector was used for imaging and analysis of tiles' surface chemistries using 5, 10 and 20 kV accelerating voltages. The Casino software [15] was applied to provide a rough estimate of the corresponding interaction volumes from which characteristic X-Rays are produced, and therefore an estimate of the depth of the oxides present. Further image analysis was undertaken using Image-J to gain an estimate of the average oxide island size and distribution [16]. Raman Spectroscopy was undertaken on both the limiter and dump plate tiles in back-scattering geometry, using a Horiba-Jobin Yvon LabRAM apparatus ( $\times 100$  objective, 0.9 numerical aperture, laser wavelength of  $514.4\text{ nm}$  and laser power of  $\sim 1\text{ mW}\mu\text{m}^{-2}$ ). The Raman Map discussed in this report was taken with a lateral resolution of  $500\text{ nm}$  and is focused on one area, which lead to the discovery of the Be-OD bond. Further information can be found in the publication by Kumar et al.

[17]. Transmission electron microscopy lamella of a cross section through the Raman mapped area (and other areas additionally) were prepared via Focused Ion Beam (FIB) on a dual beam FEI Helios. The preparation route was standard to beryllium materials [18], involving platinum surface deposition; initially with an electron beam followed by a low current ion beam, until a protective layer of  $2\text{ }\mu\text{m}$  is present. A  $30\text{ kV}$  gallium ion beam was used to trench around the area of interest, followed by undercutting. The beam current was  $22\text{ nA}$  and  $9\text{ nA}$  respectively. Lastly the area is lifted out and attached to a semi-circular omni probe copper mount, where the sample is thinned to  $\sim 100\text{ nm}$ . Further low energy cleaning occurred to achieve sub  $100\text{ nm}$  thicknesses. Samples were transferred to a Jeol-ARM200F TEM (cold-FEG, operated at  $200\text{ kV}$ ). Scanning TEM (STEM) was used predominantly and in conjunction with Energy Dispersive X-ray (EDX) in a Jeol Centurio detector and Electron Energy Loss Spectroscopy (EELS) in a Gatan Quantim GIF. Due to the limitations of EDX in detecting beryllium, EELS can be used to good effect to understand the stoichiometry's present between Be and O with future work continuing to investigate the presence of H isotopes in the low loss region of the spectra. Thermal desorption spectroscopy (TDS) data were collected on samples from similar locations along the tiles. The results are collected on a Hidden TPD workstation type 640,100. The process back heats a sample with a  $10^\circ\text{C}/\text{min}$  thermal ramp under vacuum. The gaseous species desorbed from the surface are measured via an analytical HAL/3F RC 1051-9 PIC quadrupole mass spectrometer at line-of-sight orientation for direct detection.

## 3. Experimental results and discussion

SEM studies of the beryllium surfaces were initially undertaken at lower magnifications to survey and compare the level of oxidation at different positions around JET, prior to TEM analysis. SEM voltages of 5, 10 and  $20\text{ kV}$  were used alongside the Casino software to model the depth of the interaction volume, which corresponded to  $250\text{ nm}$ ,  $400\text{ nm}$  and  $2000\text{ nm}$  respectively. Included in Table 1 is the comparison among the reactor positions of a  $20\text{ kV}$  SEM beam corresponding to  $\sim 2\text{ }\mu\text{m}$  depth. Via image analysis of EDX oxide maps, a qualitative comparison of oxide number densities which extend to  $2\text{ }\mu\text{m}$  depths is given in Table 1. Table 1 compares the outer and inner limiters with the dump plates. The outer limiters experienced lower operational temperatures than the inner limiters, whilst the dump plates experienced the highest temperatures and melt events (Fig. 1(b)). The average surface area and number density of oxide islands are greatest on the

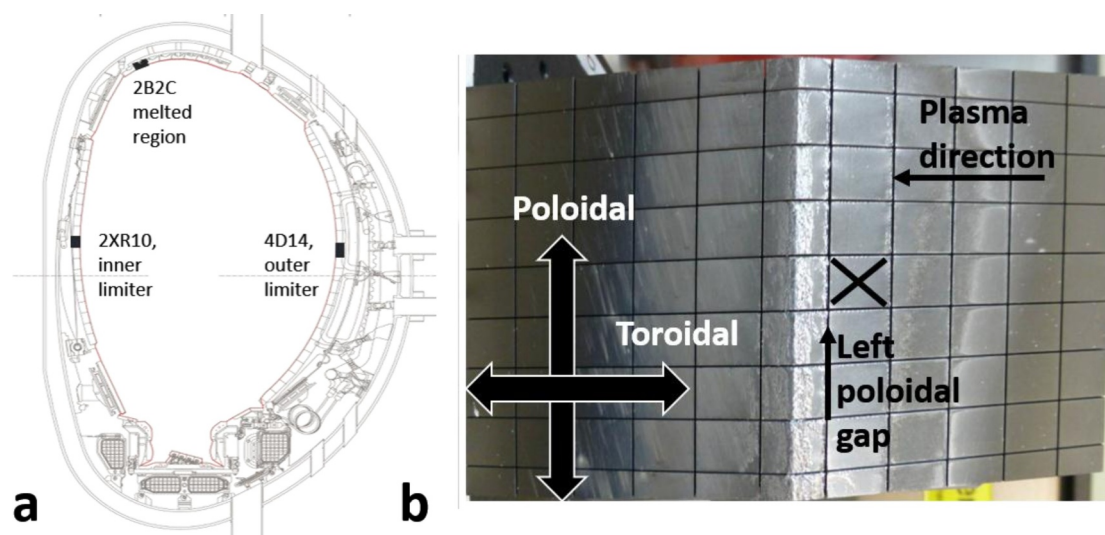


Fig. 1. Image of a) poloidal cross section of JET, showing the position of the 2B2C dump plate tile, and b) the 2B2C tile with melted central ridge. Figures include some use of colour. The reader is referred to the online version of the paper.

**Table 1**

Comparison of oxidation levels between limiter tiles and melted dump plate tile.

Position of beryllium castellation in JET	Energy Dispersive X-Ray results of oxides on the surface of beryllium materials from JET with a 20 kV accelerating voltage, interacting with ~2 $\mu\text{m}$ depths.		
	Number of oxide particles ( $\text{mm}^{-2}$ )	Average oxide particle size ( $\mu\text{m}$ )	Percentage Oxide Area ( $\text{mm}^{-2}$ )
Outer poloidal limiter eroded	57	0.17	1.0
Outer poloidal limiter deposited	20,899	8.60	18.0
Inner poloidal limiter eroded	619	0.12	7.2
Inner poloidal limiter deposited	429	0.16	7.5
Dump plate melted material	31,700	6.30	19.9

**Table 2**

List of beryllium and oxygen stoichiometries at oxidized points listed in Fig. 4.

Point in Melted Region EELS atomic-% maps (Fig. 4)	Beryllium atomic%	Oxygen atomic%
1	53.8	46.2
2	65.5	34.5
3	79.1	20.9
4	98.6	1.4
5	90.2	9.8

dump plates suggesting melt events influence oxidation behaviour. The outer poloidal limiter deposition zone, as the only position other than the dump plate nearing similar oxide island number densities and areas, occurs as an outlier. This outer limiter position experiences the coolest operational temperatures and is the most advantageous environment for deposition layers to form, with thicknesses up to  $15\mu\text{m}$ . These deposits are complex multi-layered structures of beryllium, oxygen, tungsten, nickel, nitrogen and hydrogen contaminants. In Section 3.1 EELS is used to show that the deposits have a different oxide structure to the metallic oxidation that forms under melting (Table 2).

### 3.1. Analysis of melting on fuel retention

An in-depth analysis of a specific region of the melted castellation, first studied by Raman Spectroscopy follows. Fig. 2 shows a region of melted material. This region is positioned at the left poloidal castellation gap of the dump plate tile and appears to be the result of erosion across the face of the castellation from right to left toroidally, (Fig. 1(b)) consistent with the plasma direction. The area to the right of the melted ridge has a micron sized crack network connecting islands of eroded

material. Larger macro-scale cracks are seen along all edges of the castellation, bridging regions of melted material (mounds) to the lower eroded zones. Cracking is likely in response to large thermal shocks received during operation. Presence of oxidation and the differences in thermal expansion between the oxide and S65C beryllium will increase the level of stress present in the material [7,17]. Unfortunately, marker layers complicate material chemistry due to mixing at high temperatures. Nevertheless, the oxides formed are free of nickel contaminants (Fig. 3(b)).

Raman analysis of the melted region showed the presence of the  $\text{BeO}_x\text{D}_y$  bond confirmed by comparison to Infra-Red studies of  $\text{HOBBeOH}$ ,  $\text{HBeOH}$  and  $\text{HBeOBeH}$  [19]. Further calculations using both DFT and BeO samples have confirmed the wurtzite structure, however the exact stoichiometry of the Be-OD bond is yet to be confirmed [20]. The Raman measurement was undertaken in many areas across the surface of the sample, however Be-OD retention was found solely on the melted region. The average surface roughness of the sample varied greatly, due to the limitations of the technique (attenuation of the Raman signal into the surface being ~30–50 nm in beryllium) [21], it is not apparent whether the sample's roughness is responsible for the absence of Be-OD bonding elsewhere across the sample's surface area. The Raman schematic in Fig. 2(c), shows the complex nature of the surface chemistry present without exception in all JET tiles [22]. Analysis of the Raman spectra eluded to the presence of multiple forms (up to 3 forms) of the Be-OD bond with varying stoichiometries. For further analysis of the Raman technique see Kumar et al. [17]. A Transmission Electron Microscopy (TEM) lamella of the region was produced to explore the bonding present at greater depths and confirm the structure of the oxidation. The area the lift-out was taken from is shown in Fig. 2(c) by the red box. Fig. 3 shows the extent of oxidation in the Raman analysis region, spanning ~20  $\mu\text{m}$  laterally (outlined in

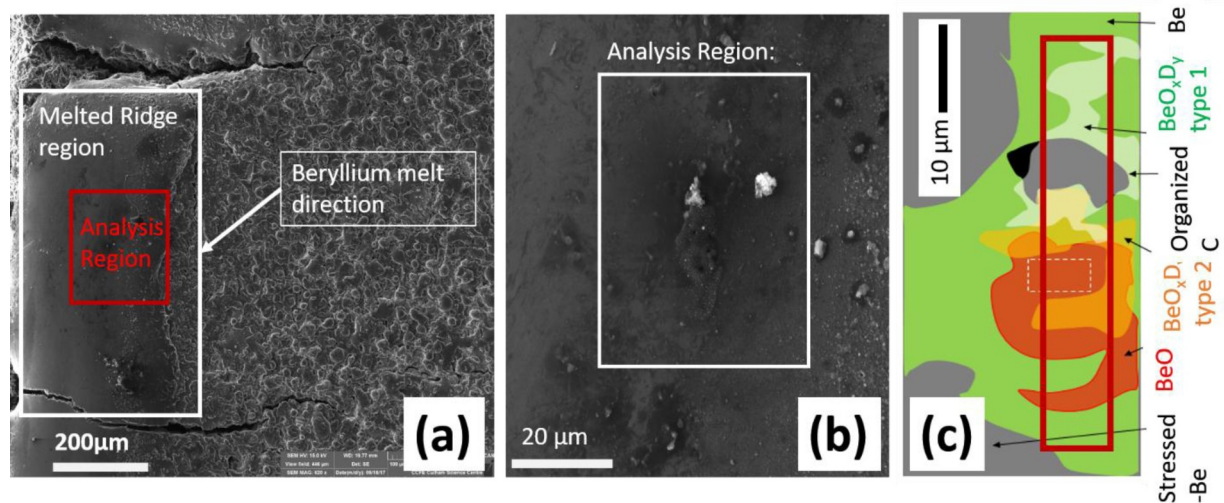


**Fig. 2.** a) SEM secondary electron image of melted ridge (left poloidal edge of the castellation), and b) the analysis region at higher magnification (0.8kx), and c) Raman schematic of the region after analysis, showing surface chemistry contributions spatially. The red box indicates the area of the TEM lift-out. Figures include some use of colour. The reader is referred to the online version of the paper.



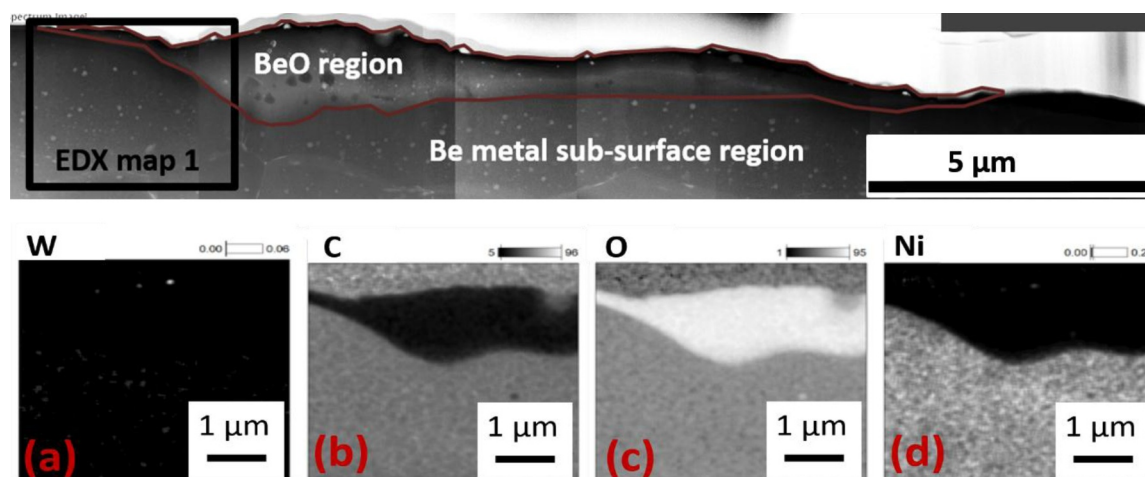


**Fig. 3.** Top) Scanning Transmission Electron Micrograph HAADF image (overview of lamella), a) background subtracted tungsten EDX map, b) background subtracted carbon EDX map, c) background subtracted oxygen EDX map, and d) background subtracted nickel EDX map. Figures include some use of colour. The reader is referred to the online version of the paper.

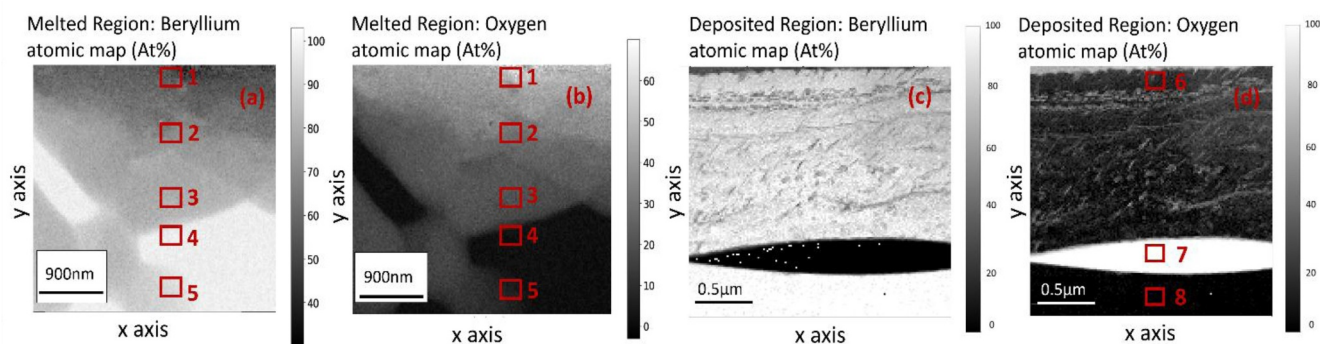


**Fig. 4.** EELS atomic percentage maps showing variations in stoichiometries of the Beryllium and oxygen edges of the melted region (a) and (b); and Beryllium and Oxygen edges from a co-deposited area of the limiter tile 2XR10 (inner poloidal limiter) (c) and (d). The extracted spectra from positions 1–5 of the melted dump plate and positions 6–8 of the codeposit are shown in Fig. 5. Figures include some use of colour. The reader is referred to the online version of the paper.

red), and at greatest depth  $\sim 2 \mu\text{m}$ . The EDX of the sample shows a clear oxidation boundary, however in-depth EELS of the region showed oxidation variability independent of grain orientation (Fig. 4).

Fig. 4(a) and (b) show the extent of oxidation present in the first  $5 \mu\text{m}$  of the melted samples' surface. The grains are clearly oxidized to different extents with 3 grains clearly seen as almost pure beryllium in Fig. 4(a) (white) and correspondingly black in Fig. 4(b). The extent of oxidation appears unrelated to the grain orientation. The extracted spectra (Fig. 5(a) and (b)), show subtle changes occurring in the fine structure. The 570 eV EELS edge maxima shifts position relative to the

grain's percentage oxidation, whilst the intensity changes in 537 eV and 543 eV peaks. The beryllium fine structure at higher oxidation, loses the 113 eV edge. Instead, under oxidation 2 new peaks at 120 and 125 eV occur with intensity varying with oxidation levels. These peak variations are consistent with the fine structures reported in [23]. Analysis of the zero-loss region may provide evidence of hydrogen isotopes in the samples [24]. Currently an edge at 19–20 eV agrees with deuterium presence in [24], however whether this is the result of deuterium; or a beryllium or oxide plasmon remains to be seen.

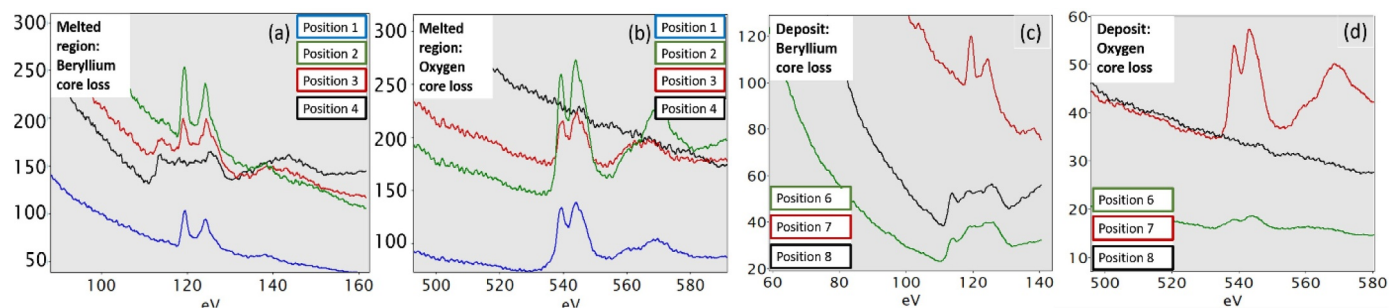


**Fig. 5.** EELS spectra extracted from: Fig. 4 showing the fine structures of the melted regions (a) and (b) and codeposited regions (c) and (d) respectively. Figure 5a) the beryllium  $\sim 113 \text{ eV}$  edge in oxidised grains (positions 1 and 2) and less oxidised grains (positions 3 and 4) and b) corresponding oxide edges at  $\sim 540 \text{ eV}$  of positions 1–4. Figure 5c) beryllium 113 eV edge of the codeposit and d) the oxide edge of the codeposit. Figures include use of colour. The reader is referred to the online version of the paper.

### 3.2. Oxidation in co-deposits

Comparatively, results from deposits formed on the inner wall limiter deposition zone (the shadowed wing region) show approximately 2  $\mu\text{m}$  of deposit formed above the surface of a surface oxide. The two oxide phases clearly show the differences in oxidation between metallic oxidation at the surface, and surface co-deposition. Fig. 5(c) and (d), show the fine edge structures extracted from position 6 (the deposit), position 7 (the crystalline oxide) and position 8 (the original beryllium surface). The fine structure of the oxide edge is significantly changed between deposits containing 20–35at% O and crystalline BeO, oxidized at the surface. The two oxide edges at  $\sim 539$  and  $545$  eV are much broader and less intense at the co-deposit site, whilst the broader peak at  $\sim 570$  eV is not visible. The co-deposit's beryllium fine structure (Fig. 5(c)) (position 6) retains greater likeness with bulk beryllium than a metallic oxide; maintaining the 113 eV edge.

The melted region occurs with grains ranging from no oxidation, to  $\sim 10\%$ ,  $\sim 20\%$ ,  $\sim 30\%$  and  $\sim 46\%$  oxidation (Table 2). The level of oxidation within the deposit is more uniform, within 20–35%. The deposited region shows an amorphous nature with ring patterns in the TEM under selected area diffraction. The deposited material appears much less ordered with at best nanometric scale horizontal regions of BeO far from stoichiometric ratios of 1:1.

### 3.3. Thermal desorption

TEM has shown eroded central regions of the limiter tiles are the most ordered. Preliminary TEM found a low density of dislocations present in the material, almost no surface oxidation, and large uniform 1–3  $\mu\text{m}$  grains in eroded regions (Fig. 6(b)). The relative microstructural simplicity of eroded materials (compared to melted and co-deposited regions), provides the best starting point for modelling desorption of fuel from TDS measurements via the Tritium Migration Analysis Program (TMAP7). Data from Ion Beam Analysis (IBA) are compiled to give a starting distribution of implanted Deuterium, with the main segment of the code being a beryllium block. Diffusion is enabled throughout the block structure and recombination limited release governs at the surface. Agreement between experimental data and the code has been successful, however on application of the same approach to the deposited material, almost no agreement stands between the desorption peak position and the modelled result. A similar experience has occurred with the oxidation seen in melted material. Early efforts to apply a surface binding energy to the oxide equivalent to that of the Be-OD bond energy have been attempted. The comparative raw data of desorption between an eroded region, a melted region and a deposited region of the 2010–12 campaign are given for completeness (Fig. 7). The melted region has comparably lower retention levels than

those seen in both the eroded and deposited regions. The deposited material remains the highest mechanism of retention. The highly porous sedimentary like structure of the deposit (Fig. 6(a)) with respect to the eroded surface, suggests that the desorption kinetics of the material are significantly altered from crystalline beryllium. It is suggested physical processes such as surface area and surface tension have greater effect on the trapping behaviour in these materials than diffusivities. Further investigation of these traits with TMAP7 is planned and will be published in the future. From the raw data, the desorption peak position of the melted material has shifted to higher temperatures of  $\sim 825$  K, than its eroded counterpart. The deposited material has an initial release at  $\sim 675$  K followed by a much larger release at 925 K; compared to the single peak release of both the eroded and melted materials. Finally, desorption in the deposited material is incomplete at the maximum operating temperature of the TDS, prior to beryllium evaporation.

## 4. Conclusion

The first results of EELS analysis following the discovery of the Be-OD bond with Raman have been reported [17]. The EELS results compliment those seen with Raman. Complex oxidation is present in the sample with two or more phases present. Ongoing modelling work, and EELS with standardised BeO materials is occurring to determine the influence of deuterium presence on the EELS fine structure and enable further stoichiometric characterisation of the  $\text{BeO}_x\text{D}_y$  bond. EELS unlike Raman can view the sub-surface structure beyond 50 nm. Early application of these microstructural findings to desorption data continue. The results of desorption modelling will be the subject of future publication. Whilst the discovery of the Be-OD bond is interesting, overall retention resulting from its formation appears limited in JET due to low levels of melted material. In 2010–11 (ILW1)  $\sim 19$  g of melted material is estimated in the dump plate region, 134 g in 2012–13 (ILW2), and  $\sim 30$  g in 2014–15 (ILW3). Retention in the first 0–3  $\mu\text{m}$  of these limited wall areas is unlikely to significantly contribute to overall hydrogen retained across the reactor. Nevertheless, if operation conditions in ITER enable higher wall temperatures for longer periods in steady state, with greater ELMs and displacement events, oxide formation and chemical retention could be substantial [25]. The raw TDS data suggests the presence of an oxide bond at the surface has led to higher desorption peak temperatures relative to eroded surface regions. Post dynamic out-gassing; a situation could exist under higher temperature operation, where an increase in diffusion is seen into the bulk [25], alongside creation of a surface barrier. A previous study [26] found oxidation did not lead to a desorption barrier. Whilst JET's desorption results show some similarities, with similar peak desorption temperatures between the melted region and their oxidised samples (with a reasonable range of uncertainty) [27]; no early release is seen, enabling the possibility of barrier behaviour. Other factors such as cracking could decrease retention overall and expedite release mechanisms. The overall outcome of chemical bond formation on desorption is therefore complex. JET's current TDS data shows melted materials retain lower levels of deuterium than co-deposited counterparts. However, the desorption appears incomplete and a tail into higher temperatures could exist with the possibility of longer and higher temperature programmed desorption required, which could affect ITER baking operations.

### Funding statement

“This work has been carried out within the framework of the EUROfusion Consortium and has received funding from the Euratom research and training programme 2014–2018 under grant agreement no 633053. The views and opinions expressed herein do not necessarily reflect those of the European Commission.”

“The research used UKAEA's Materials Research Facility, which has

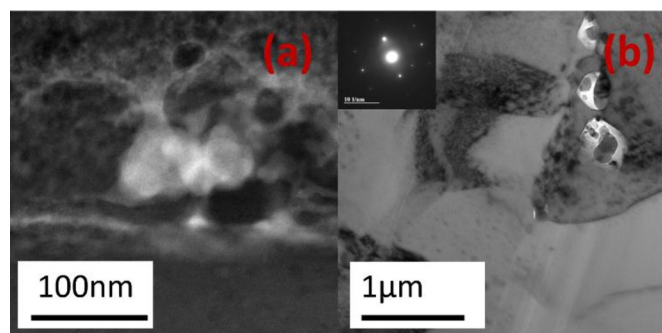


Fig. 6. a) Porous structure of the deposit, showing nanoscale voids potentially enabling  $\text{D}_2$  gas retention, b) TEM bright field image of eroded material, showing gas filled cavities along grain boundaries in crystalline metallic beryllium. Figures include some use of colour. The reader is referred to the online version of the paper.

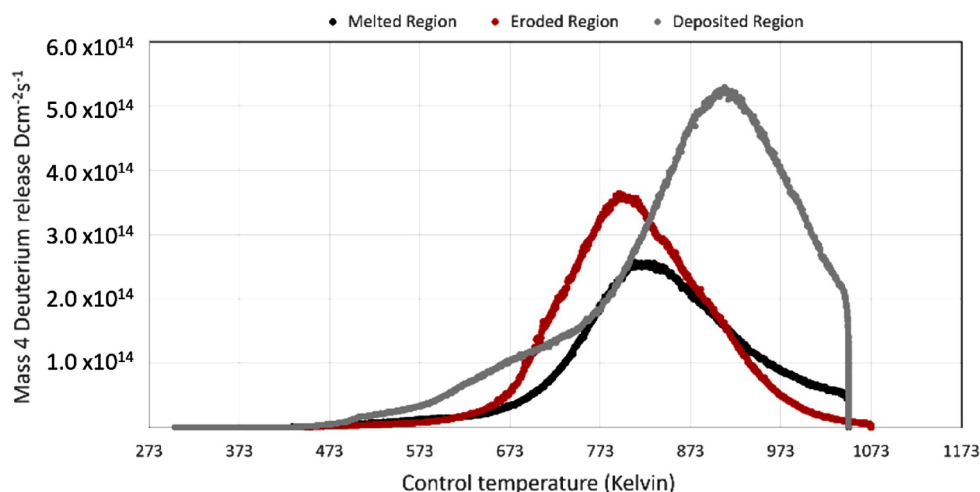


Fig. 7. Thermal Desorption data of an eroded, melted and deposited castellation. The deposited region release is limited by the maximum operating temperature of the TDS system ( $\sim 800^\circ\text{C}$ ) due to beryllium safety requirements. Figures include some use of colour. The reader is referred to the online version of the paper.

been funded by and is part of the UK's National Nuclear User Facility and Henry Royce Institute for Advanced Materials."

### Supplementary materials

Supplementary material associated with this article can be found, in the online version, at [doi:10.1016/j.nme.2019.02.022](https://doi.org/10.1016/j.nme.2019.02.022).

### References

- [1] K. Heinola, A. Widdowson, J. Likonen, E. Alves, N. Barradas, S. Brezinsek, N. Catarino, P. Coad, S. Koivuranta, S. Krat, G.F. Matthews, M. Mayer, P. Petersson, J.E.T. Contributors, Long-term fuel retention in JET ITER-like wall, *Phys. Scr.* T167 (2016) 1–7.
- [2] J. Roth, R. Doerner, M. Baldwin, T. Dittmar, H. Xu, K. Sugiyama, M. Reinelt, C. Linsmeier, M. Oberkofler, Oxidation of beryllium and exposure of beryllium oxide to deuterium plasmas in PISCES B, *J. Nucl. Mater.* 438 (Suppl) (2013) 1044–1047.
- [3] D.W. Aylmore, S.J. Gregg, W.B. Jepson, The high temperature oxidation of beryllium. Part I. In dry oxygen, *J. Nucl. Mater.* 2 (2) (1960) 169–175.
- [4] A. Allouche, Quantum modeling of hydrogen retention on partially oxidized beryllium, *J. Nucl. Mater.* 415 (1 Suppl) (2011) S721–S723.
- [5] S. Zalkind, M. Polak, N. Shamir, Adsorption of hydrogen on clean and oxidized beryllium studied by direct recoil spectrometry, *Appl. Surf. Sci.* 115 (3) (1997) 273–278.
- [6] S. Zalkind, M. Polak, and N. Shamir, "The adsorption of H<sub>2</sub>O vs O<sub>2</sub> on Beryllium," vol. 385, pp. 318–327, 1997.
- [7] D.A. Petti, G.R. Smolik, R.A. Anderl, On the mechanisms associated with the chemical reactivity of Be in steam, *J. Nucl. Mater.* 283–287 (Part II) (2000) 1390–1395.
- [8] S. Zalkind, M. Polak, N. Shamir, Effects of preadsorbed hydrogen on the adsorption of O<sub>2</sub>, CO and H<sub>2</sub>O on beryllium, *Surf. Sci.* 539 (1–3) (2003) 81–90.
- [9] S. Zalkind, M. Polak, N. Shamir, Oxidation of ion-bombarded vs. annealed beryllium, *Surf. Sci.* 513 (3) (2002) 501–510.
- [10] A. Allouche, M. Oberkofler, M. Reinelt, C. Linsmeier, Quantum modeling of hydrogen retention in beryllium bulk and vacancies, *J. Phys. Chem. C* 114 (8) (2010) 3588–3598.
- [11] A. Allouche, Quantum modeling of hydrogen retention on partially oxidized beryllium, *J. Nucl. Mater.* 415 (1 Suppl) (2011) S721–S723.
- [12] A. Widdowson, A. Baron-Wiechec, P. Batistoni, E. Belonohy, J.P. Coad, P. Dinca, D. Flammini, F. Fox, K. Heinola, I. Jecu, J. Likonen, S. Lilley, C.P. Lungu, G.F. Matthews, J. Naish, O. Pompilian, C. Porosnicu, M. Rubel, R. Villari, Experience of handling beryllium, tritium and activated components from JET ITER like wall, *Phys. Scr.* T167 (1) (2016) 014057.
- [13] M. Rubel, J.P. Coad, A. Widdowson, G.F. Matthews, H.G. Esser, T. Hirai, J. Likonen, J. Linke, C.P. Lungu, M. Mayer, L. Pedrick, C. Ruset, Overview of erosion-deposition diagnostic tools for the ITER-Like Wall in the JET tokamak, *J. Nucl. Mater.* 438 (Suppl) (2013) S1204–S1207.
- [14] C. Lungu, I. Mustata, V. Zaroschi, A. Lungu, A. Anghel, P. Chiru, M. Rubel, P. Coad, G. Matthews, Beryllium coatings on metals for marker tiles at JET: development of process and characterization of layers, *Physica Scripta* T128 (2007) 157–161.
- [15] P. Hovington, D. Drouin, R. Gauvin, CASINO: a new Monte Carlo code in C language for electron beam interaction -part I: description of the program, *Scanning* 19 (1) (2006) 1–14.
- [16] J. Schindelin, I. Arganda-Carreras, E. Frise, V. Kaynig, M. Longair, T. Pietzsch, S. Preibisch, C. Rueden, S. Saalfeld, B. Schmid, J.-Y. Tinevez, D.J. White, V. Hartenstein, K. Eliceiri, P. Tomancak, A. Cardona, Fiji: an open-source platform for biological-image analysis, *Nat. Methods* 9 (7) (Jul. 2012) 676–682.
- [17] M. Kumar, C. Makepeace, C. Pardanaud, E. Hodille Y. Ferro, C. Martin, P. Roubin, A. Widdowson, T. Dittmar, Ch. Linsmeier, C.P. Lungu, C. Porosnicu, I. Jecu, P. Dinca, M. Lungu, O.G. Pompilian, Identification of BeO and BeOx/Dy in melted zones of the JET Be limiter tiles: raman study using comparison with laboratory samples, *Nucl. Mater. Energy* 17 (2018) 295–301.
- [18] M. Schaffer, B. Schaffer, Q. Ramasse, "Sample preparation for atomic-resolution STEM at low voltages by FIB," vol. 114, pp. 62–71, 2012.
- [19] C.A. Thompson and L. Andrews, "Reactions of laser ablated Be atoms with H<sub>2</sub>O: infrared spectra and density functional calculations of HOBeOH, HBeOH, and HBeOBeH," vol. 1, no. 96, pp. 12214–12221, 1996.
- [20] E.A. Hodille, Y. Ferro, Z.A. Piazza, C. Pardanaud, Hydrogen in beryllium oxide investigated by DFT: on the relative stability of charged-state atomic versus molecular hydrogen, *J. Phys. Condens. Matter* 30 (30) (Aug. 2018) 305201.
- [21] C. Pardanaud, C. Martin, C. Pardanaud, C. Martin, and P. Roubin, "Raman Microscopy: a suitable tool for characterizing surfaces in interaction with plasmas in the field of nuclear fusion," in *Raman Spectrosc. Appl.*, p. 30. 2017.
- [22] C. Pardanaud, M.I. Rusu, G. Giacometti, C. Martin, Y. Addab, P. Roubin, C.P. Lungu, C. Porosnicu, I. Jecu, P. Dinca, M. Lungu, O.G. Pompilian, R. Mateus, E. Alves, and M. Rubel, "Raman microscopy investigation of beryllium materials," 2016.
- [23] H.H. Madden, R. Landers, G.G. Kleiman, D.M. Zehner, Oxygen-induced changes in electron-energy-loss spectra for Al, Be and Ni, *J. Vac. Sci. Technol. A* 17 (5) (1999) 2719–2730.
- [24] V.P. Afanas'ev, A.S. Gryazev, P.S. Kaplya, M. Köppen, O.Y. Ridzel, N.Y. Subbotin, P. Hansen, Investigation of deuterium implantation into beryllium sample by electron energy loss spectroscopy, *J. Phys. Conf. Ser.* 891 (1) (Nov. 2017) 012303.
- [25] R.W. Conn, R.P. Doerner, J. Won, Beryllium as the plasma-facing material in fusion energy systems—experiments, evaluation, and comparison with alternative materials, *Fusion Eng. Des.* 37 (4) (1997) 481–513.
- [26] P. Zhang, J. Zhao, B. Wen, Retention and diffusion of H, He, O, C impurities in Be, *J. Nucl. Mater.* 423 (1–3) (2012) 164–169.
- [27] J. Roth, W.R. Wampler, M. Oberkofler, S. van Deusen, S. Elgeti, Deuterium retention and out-gassing from beryllium oxide on beryllium, *J. Nucl. Mater.* 453 (1–3) (2014) 27–30.